Remodeling of the interdomain allosteric linker upon membrane binding of CCTα pulls its active site close to the membrane surface

Received for publication, June 18, 2019, and in revised form, August 18, 2019 Published, Papers in Press, September 4, 2019, DOI 10.1074/jbc.RA119.009850

Daniel G. Knowles[‡1], **Jaeyong Lee**[‡], **Svetla G. Taneva**[‡], **and Rosemary B. Cornell**[‡§2]

From the Departments of [‡]*Molecular Biology and Biochemistry and* [§]*Chemistry, Simon Fraser University, Burnaby, British Columbia V5A 1S6, Canada*

Edited by George M. Carman

The rate-limiting step in the biosynthesis of the major membrane phospholipid, phosphatidylcholine, is catalyzed by CTP: phosphocholine cytidylyltransferase (CCT), which is regulated by reversible membrane binding of a long amphipathic helix (domain M). The M domain communicates with the catalytic domain via a conserved ~20-residue linker, essential for lipid activation of CCT. Previous analysis of this region (denoted as the αE_C/J) using MD simulations, cross-linking, mutagenesis, and solvent accessibility suggested that membrane binding of domain M promotes remodeling of the αE_C/J into a more compact structure that is required for enzyme activation. Here, using tryptophan fluorescence quenching, we show that the allosteric linker lies superficially on the membrane surface. Analyses with truncated CCTs show that the αE_C/J can interact with lipids independently of the M domain. We observed strong FRET between engineered tryptophans in the αE_C/J and vesicles containing dansyl-phosphatidylethanolamine that depended on the native J sequence. These data are incompatible with the extended conformation of the αE helix observed in the previously determined crystal structure of inactive CCT but support a bent αE helix conformation stabilized by J segment interactions. Our results suggest that the membrane-adsorbed, folded allosteric linker may partially cover the active site cleft and pull it close to the membrane surface, where cytidyl transfer can occur efficiently in a relatively anhydrous environment.

Allosteric linkers propagate signals between effector-binding regulatory domains and functional domains of proteins by modulating their conformation and dynamics. Allosteric linkers generally possess conserved sequences that encode favored folding pathways that are triggered by effector binding events in the regulatory domain (1). Regulatory linker segments can be ordered and bound to one or more domains in one functional state and freed to equilibrate between other favored states and new interactions in a second functional state (2–5). Our work on the lipid-regulated enzyme, CTP:phosphocholine cytidylyltransferase, α isoform (CCTα)[3] suggests that it also contains an allosteric linker whose function relies on its malleability and sequence conservation that stipulates a hierarchical pathway of conformational transitions down an energy landscape, where folding intermediates populate increasingly lower-energy states to the fully functional state (1).

CCT is an intriguing enzyme of phosphatidylcholine metabolism that is regulated allosterically by membrane binding. In effect, its "ligand" is a membrane surface, and not just any membrane. *In vitro* CCT binds preferentially to membranes that are relatively depleted in PC by recognition of lipid-packing defects and higher negative charge that are features of PC-depleted membrane surfaces (6). In most cells, the CCTα isoform is localized in the nucleus and binds to the inner nuclear membrane in response to conditions such as oleic acid loading, phosphatidic acid accumulation, or changes in the PE/PC ratio (7–11). Membrane binding activates the enzyme and restores PC synthesis and membrane PC content. The CCT membrane-binding M domain folds into a long amphipathic helix on such surfaces and creates a stable association (Fig. 1). The binding triggers shifts in the conformational equilibrium that propagates from domain M to the catalytic (C) domain to increase catalytic efficiency by about 200-fold (6, 12).

Bridging the C and M domains is an allosteric linker we refer to as the αE_C/J (residues 216–234, mammalian numbering; Fig. 1) that is highly conserved across phyla (13), contains both charged and nonpolar residues, and is lacking in cytidylyltransferases that are not lipid-regulated. In the companion paper (13), we showed via analysis of the impacts of mutations in this region on CCT activity that the αE_C/J is vital for lipid-dependent activity. Cross-linking studies suggested that the activity relies on the malleability of the αE (14). The modular nature is evident in the different conformations adopted in solved crystal structures of this homodimeric enzyme. In the inactive soluble

This work was supported by a grant from the Canadian Institutes for Health Research (to R. B. C.). The authors declare that they have no conflicts of interest with the contents of this article.
This article contains Table S1 and Figs. S1–S9.

[1] Present address: Animal Health Branch, British Columbia Ministry of Agriculture, Abbotsford, British Columbia V3G 2M3, Canada.
[2] To whom correspondence should be addressed: Dept. of Molecular Biology and Biochemistry, Simon Fraser University, Burnaby, British Columbia V5A 1S6, Canada. Tel.: 778-782-3709; E-mail: cornell@sfu.ca.

[3] The abbreviations used are: CCT, CTP:phosphocholine cytidylyltransferase; domains C and M, catalytic and membrane-binding domains, respectively; AI, auto-inhibitory; POPC, 1-palmitoyl-2-oleoyl-*sn*-glycero-3-phosphocholine; PG, phosphatidylglycerol; PE, phosphatidylethanolamine; PC, phosphatidylcholine; LPC, 1-palmitoyl lysophosphatidylcholine; Br-PC, dibrominated phosphatidylcholine; SUV, small unilamellar vesicle; PDB, Protein Data Bank; FPLC, fast protein liquid chromatography; DOPC, 1,2-dioleoyl-*sn*-glycero-3-phosphocholine; DOPE, 1,2-dioleoyl-*sn*-glycero-3-phosphoethanolamine; nSMase2, neutral sphingomyelinase; NSL, nuclear localization signal.

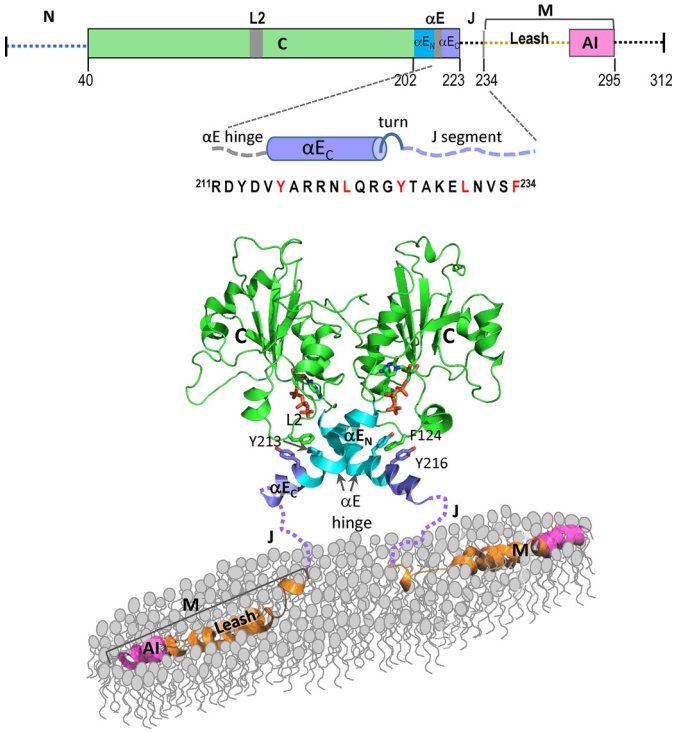

Figure 1. Structure of CCTα-312. *Top*, domain map. The N-terminal 40 residues are disordered. The C domain highlights loop L2, which contains Lys-122, a target of regulation by the AI (*pink*) helix. The allosteric linker region (*blue*) is subdivided into N-terminal (αE_N) and C-terminal (αE_C) helices with an intervening αE hinge (*gray box*). The αE_C/J region is enlarged, and its sequence is provided, with the residues we substituted with tryptophan indicated in *red*. The M domain is depicted as in its soluble form: a disordered "leash" followed by the AI helix (*pink*). *Bottom*, structure of residues 40–288. The model for the catalytic dimer is one snapshot from a molecular dynamics simulation (14) showing one of the four common bent conformations for the αE helices in the absence of the AI helices. The substrate CTP (*stick representation*) occupies the active site. The aromatic cluster composed of two residues from the αE and one from loop L2 is *highlighted* with *stick representations*. The image for the M-helix is based on PDB entries 1PEI and 1PEH, depicting the leash and AI segment in their membrane-bound (helical) conformation. The J segment structure (*dashed lines*) is unknown.

form (CCT_{sol}), the αE is a 22-residue unbroken helix extending from the active site and is constrained by formation of a four-helix complex consisting of two αE and two auto-inhibitory (AI) helices contributed from the M domain.

The J segment is not visible in this structure, suggesting disorder. In the structure of the truncated CCT-236 that lacks domain M (and the AI) but includes the allosteric linker, only the N-terminal 14 or 15 residues of the two αE helices (αE_N (Thr-202 to Asp-212) and αE hinge (Tyr-213 to Val-215) are resolved, whereas neither the αE_C (Tyr-216 to Arg-223) nor J segment (Tyr-225 to Phe-234) are visible, suggesting that they are both disordered. Although no electron density was obtained for the J segment in these high-resolution structures, the electron density for a low-resolution (8 Å) crystal of a CCT tetramer (PDB code 4MVD) defined the residues comprising the αE_C/J as helical. In two of the four chains, the αE_C and J segment were linked by a sharp ~75° turn at ^{223}RGY^{225} (15). These data suggest a helical preference for the αE and J segment that is interrupted by hinges in the middle of the αE (αE hinge) and between the αE_C and J segment. But acquisition of stable helix structure may require a template upon which to fold.

Recent molecular dynamics simulations also revealed the plasticity of the αE hinge. In the simulations of CCT-236, residues of the αE_C and J segment showed a high degree of malleability and divergence from the starting structure (15). In simulations of residues 40–223 missing the J segment and M domain, the αE_C was externally restrained to remain helical, but the rest of the αE was unrestrained. The αE_N pair retained helical structure and interhelical contacts throughout the 1-μs simulations, but the hinge at residues 212–215 sampled many conformations (14). The most long-lived conformers (up to 700 ns) displayed a prolonged sharp bend at the hinge that brought the C terminus of the αE_C proximal to the active site and loop L2. The bent αE helix conformations showcased a new interdomain aromatic cluster involving two tyrosines within or proximal to the αE hinge and a phenylalanine in loop L2 of the active site.

In vitro support for αE malleability as essential to drive CCT activation was provided by "straight-jacketing" the αE helices with chemical cross-links (14). When the helices were constrained from bending, activation of the membrane-bound enzyme (CCT_{mem}) was impaired. The activity-promoting impact of mutations in the αE hinge that destabilize interactions between the αE helix pair underscored the importance of helix αE malleability (13). The solvent accessibility of residues in the αE hinge in CCT_{mem} was consistent with a hinge that exists within a folded ensemble (13). The working hypothesis is that the membrane-triggered displacement of the AI helices frees the αE_C to sample other conformations, including ones more productive for catalysis. Based on the conserved and amphipathic nature of the αE_C/J segment and its proximity to domain M, we further hypothesize that the fully active conformation of this sequence includes an association with membranes as a compact, folded unit. Such an association could stabilize a rearrangement of the αE helices that would dock the catalytic domain close to the membrane surface.

In the present work, we show that the αE_C and J segment interact with the membrane surface in CCT_{mem}, and both can do so independently of the adjacent M domain. FRET analysis between Trp donor sites in CCT and a lipid acceptor shows that the active site is pulled closer to the membrane surface than would be predicted in a model with the αE helices fully extended. These data provide evidence for a compact structure of the αE and J segment that together comprise an allosteric linker whose conformational ensemble is constrained and directed by membrane association. Last, we address how catalysis could be enhanced by drawing the active site close to the membrane surface.

Results

Brominated PC (Br-PC) quenching of single-Trp variants reveals a superficial association of the allosteric linker with membranes

As there is no solved structure of lipid-bound CCT, the orientation of the αE_C/J relative to the membrane surface is not known. To assess whether sites in this segment interact with the membrane surface, we explored the fluorescence quenching of

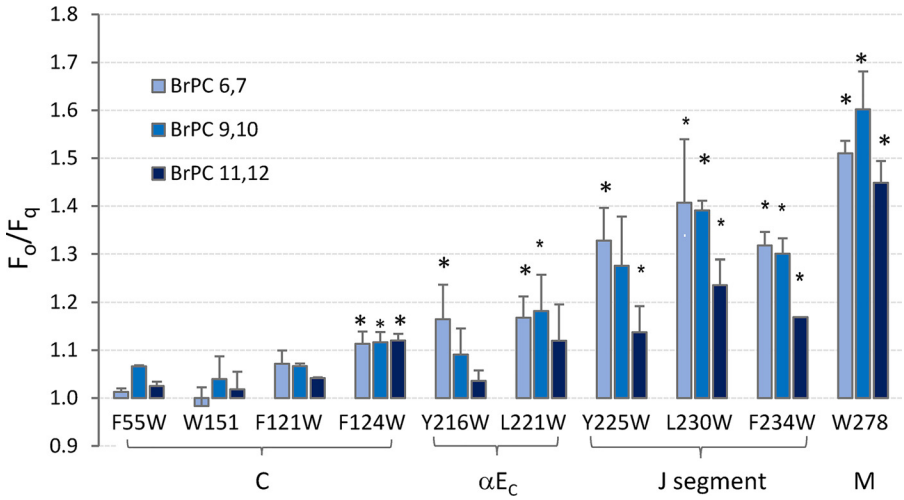

Figure 2. The αE_C and J segment in CCT_{mem} interact with membranes superficially. The fluorescence of CCT-312 with single Trps at the indicated positions was monitored in the presence of vesicles composed of POPC/egg PG (1:1) (unquenched; F_o) or dibrominated PC/egg PG (1:1) (quenched; F_q). The [CCT] was 3 μM, and the [lipid] was 450 μM. Spectra were corrected for lipid blanks, and the peak fluorescence intensities were obtained. Individual representative spectra are found in Fig. S1. Data are means ± average deviation (*error bars*) of 2–5 independent determinations. The *large* and *small asterisks* indicate significant *p* values (≤0.01 and 0.05, respectively) compared with quenching of F55W by the respective Br-PC. Single-Trp constructs are derived from a CCT-312-His Δ12–16 background with native Trps removed (W151F; W278F). "W151" and "W278" retain the indicated single native Trp.

engineered tryptophans by vesicles containing Br-PC. The preparation and analysis of the impact of many of the αE/J-engineered Trps on CCT activity and thermal stability were presented in the companion paper (13). In addition, we analyzed single Trps engineered into the catalytic domain at F121W and F124W that were characterized previously (14). The Trp substitutions did not affect the stability of the catalytic domain fold (Table S1). The Trps engineered into αE/J did not impair the interaction of the M domain with membrane vesicles. All active αE/J Trp variants had approximately the same affinity as the WT CCT for the highly curved vesicles used in the fluorescence experiments (13).

We probed Trp quenching by PCs brominated at the 6,7-, 9,10-, or 11,12- positions of the acyl chain. Quenching by Br-PC requires van der Waals contact of the excited Trp and bromine on the acyl chain (16). In keeping with published data using domain M peptides (17), Trp-278 was strongly quenched by all three depths of bromine quenchers in the context of CCT-312, with the strongest impact using 9,10-Br-PC (Fig. 2). These data support a stable interaction between the vesicles and domain M. In contrast, Trp-55 at the N terminus of the catalytic domain was not significantly quenched by any Br-PC vesicles. Trp-151 near the active site was also not quenched. These results provide evidence that Br-PC quenching monitors the persistence of Trp residue–membrane interactions and that random collision with vesicles does not contribute significantly to quenching.

Trps at the N terminus (Trp-225), middle (Trp-230), and C terminus (Trp-234) of the J segment were moderately quenched by Br-PC, most prominently at the shallower 6,7- and 9,10-positions (Fig. 2). Interestingly, Trp-216 and Trp-221 were weakly quenched, despite their location in the αE_C. Even more surprisingly, Trp-124 in loop L2 of the catalytic domain was quenched beyond background levels by the Br-PC. These data suggest that the conformational ensemble for CCT_{mem} includes a population where the allosteric linker situates superficially at the membrane surface and where Phe-124 in loop L2 makes transient excursions toward the membrane surface. The Trps in the αE_C/J remain accessible to acrylamide, except for the Trp at residue 216, near the αE hinge, which is buried in CCT_{mem} (13).

We attempted to interrupt the membrane interaction of the allosteric linker by mutation to probe whether this association is required for signaling from the bound M domain to the active site. We tested the effects of three mutants on quenching by Br-PC: 3Φ (L230A/V232A/F234A) to reduce the hydrophobicity, 3R (R219Q/R223Q/K228Q) to reduce the electrostatic drive, and 3Aro (Y216A/Y225A/F234A) to eliminate the aromatic pull toward the bilayer interface (Fig. 3*A*). The transition temperatures for unfolding of these variants were the same as the parent CCT from which they were derived, indicating proper domain C folding (49.8 ± 0.2 °C for the four CCTs). The mutations devastated the enzyme activity (Fig. 3*B*), confirming the strong dependence of catalytic function on the native linker sequence (13). We did not assay the activity of the triple aromatic variant, as we knew that the substitution of just one of the sites, Y216A, was strongly inactivating (13). The interaction with the membrane was monitored by Br-PC quenching of either engineered Trp-225 or Trp-221. To our surprise, none of the mutations reduced the quenching of Trp-225 or Trp-221 (Fig. 3*C*). These results suggest that either the linker interaction with the membrane involves multiple disperse interactions that survive the loss of a few sites or that the method of Br-PC quenching of engineered Trps is not accurately reporting a binding event for the linker. The allosteric linker is in close proximity to the M domain with its known membrane-anchoring properties. Could the bound M domain and the engineered Trps be pulling the linker to the surface at the engineered site? To address this concern, we probed whether the linker has membrane-binding properties independent of the M domain and engineered Trps.

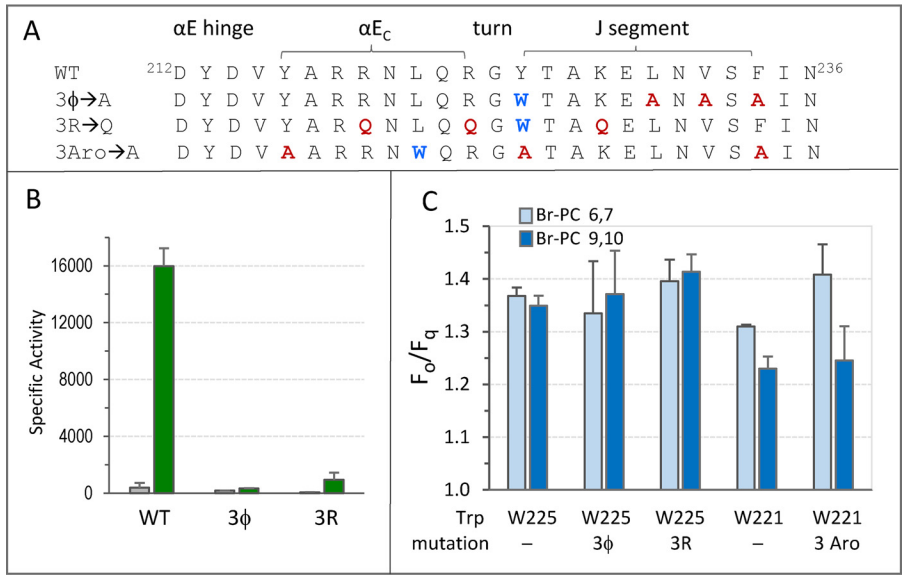

Figure 3. Effect of mutations that change the charge or hydrophobicity of the allosteric linker on membrane proximity and enzyme activity. *A*, sequence of the allosteric linker, positions of Trp mutations to monitor fluorescence, and other sets of mutations to alter properties of the linker. *B*, the activities (nmol of CDP-choline formed/min/mg of CCT) of the indicated CCTs were determined under standard conditions in the absence (*gray*) or presence (*green*) of 0.2 mM PC/PG (1:1) SUVs. Data are means ± range (*error bars*) of two independent determinations. "3ϕ" and "3R" are derived from a CCT-312-His Δ12–16 background with one native Trp removed (W278F), whereas "WT" retains both native Trps (Trp-151 and -278). *C*, the fluorescence of CCT-312 with single Trps at the indicated positions was monitored in the presence of vesicles composed of POPC/egg PG (1:1) (unquenched; F_o) or dibrominated PC/egg PG (1:1) (quenched; F_q). The [CCT] was 3 μM, and the [lipid] was 450 μM. Spectra were corrected for lipid blanks, and the peak fluorescence intensities were obtained. Data are means ± range of two independent determinations. Individual representative spectra are found in Fig. S2. Single-Trp constructs are derived from a CCT-312-His Δ12–16 background with native Trps removed (W151F; W278F).

Lipid interactions with CCT-236 implicate the αE$_C$/J segment as a membrane-binding region

CCT-236 is truncated at the boundary between the allosteric linker and domain M. It has weak constitutive activity, but we have documented that its V_{max} can be elevated ~2-fold by lipid vesicles (13). By contrast, the V_{max} for full-length CCT is elevated >30-fold by lipids. In the companion paper (13) we showed that deletion of residues 227–232 of the J segment decreased the activity of CCT-236 both in the absence and presence of lipids, but the mutant was still activated ~2-fold by lipids (Fig. 3*B* of Ref. 13). We examined the membrane binding of CCT-236 with a native J sequence or with the J segment deletion, using Br-PC quenching of an engineered Trp-225 at the start of the J segment. We found that Br-PC quenching of Trp-225 was even stronger in CCT-236 than in CCT-312 (Fig. 4). Trp-151 in the active site, a negative control, showed no quenching. Surprisingly, the quenching of Trp-225 in CCT-236 was not reduced by deletion of J segment residues 227–232, but was even enhanced (Fig. 4). This suggests that the J segment, although important for catalytic function, is not required for association of CCT-236 with membranes. Rather, membrane association involves alternative or additional residues (*e.g.* residues in the αE$_C$).

We then analyzed CCT-236 lipid association using an alternative method that does not rely on engineering tryptophans, which could impart membrane partitioning bias. We used gel filtration of CCTs containing only native Trps in the presence or absence of activating micelles (lyso-PC 16:0). These micelles activate CCT-236 and the 236 ΔJ deletion mutant as effectively as sonicated lipid vesicles (Fig. 5*A*). They are also effective but weaker activators of full-length CCT and CCT-312. To probe

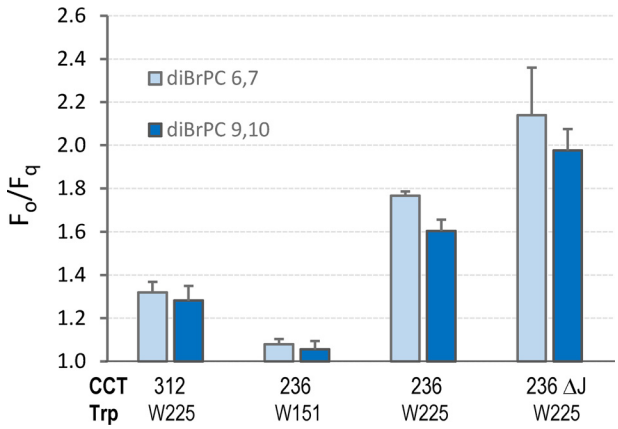

Figure 4. CCT-236 interacts with lipid vesicles independently of the linker. The fluorescence of CCT-312 or CCT-236 with single Trps at the indicated positions was monitored in the presence of vesicles composed of POPC/egg PG (1:1) (unquenched; F_o) or dibrominated PC/egg PG (1:1) (quenched; F_q). The [CCT] was 3 μM, and the [lipid] was 450 μM. Spectra were corrected for lipid blanks, and the peak fluorescence intensities were obtained. Data are means ± average deviation (*error bars*) of 3–4 independent determinations. Individual representative spectra are found in Fig. S3. Single-Trp constructs are derived from a CCT-312-His Δ12–16 background with native Trps removed (W151F; W278F) or a His-CCT-236 Δ12–16 background with the native Trp removed (W151F).

whether Superdex-200 chromatography can distinguish CCT that is free *versus* micelle-bound, we first examined a CCT with domain M. We used CCT-312Δ32 with a shortened domain M as it retained better solubility than the CCT-312 construct with a full-length M domain during concentration prior to gel filtration. This construct retains the AI helix but is missing the leash portion of domain M, residues 238–269. In the absence of lipid, CCT-312Δ32 eluted as two populations, one with a mass approximating a dimer, slightly larger than the albumin stan-

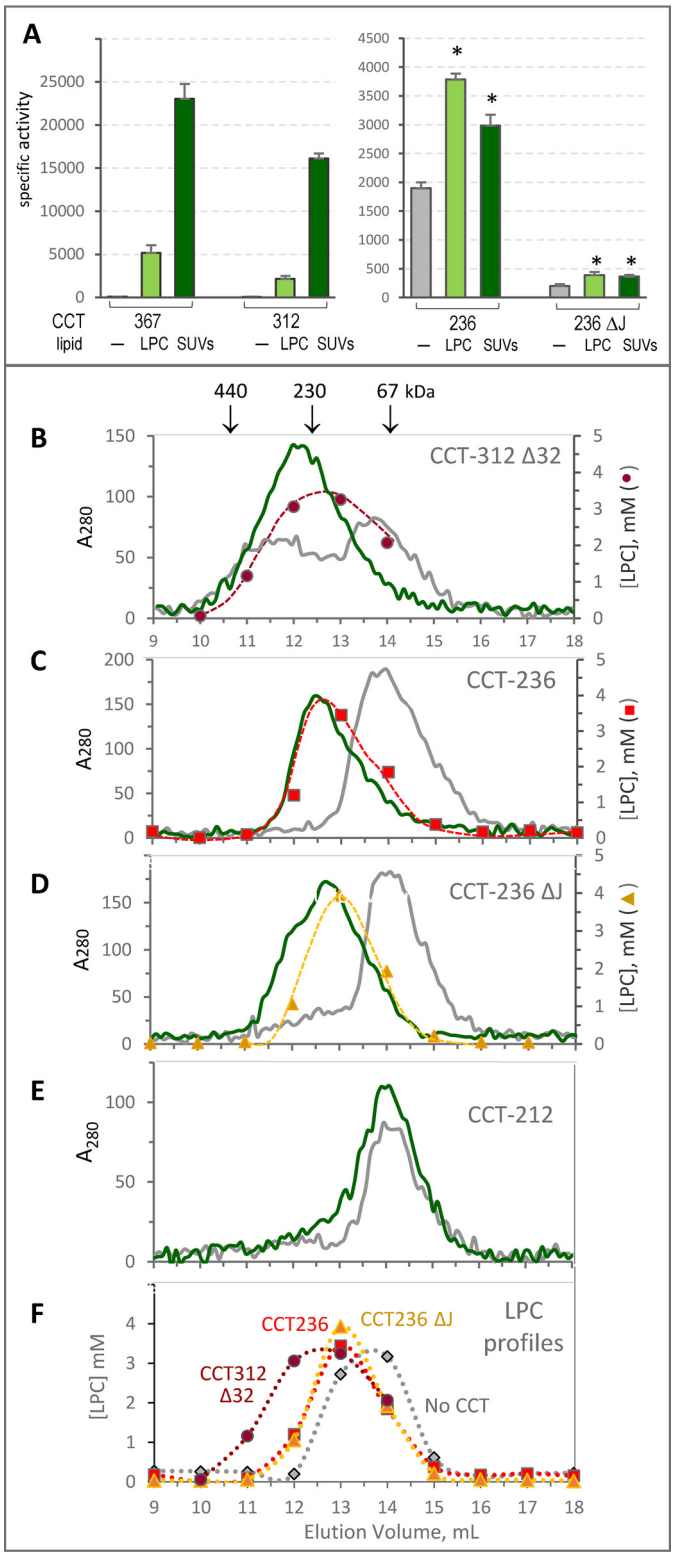

Figure 5. Lipid affinity of αE_C/J can be independent of domain M interaction with membranes. *A*, activation of CCTs by LPC (16:0). CCTs were incubated with buffer, 10 μM LPC, or 100 μM egg PC/egg PG (1:1) SUVs for 5 min prior to assay under conditions optimal for the indicated CCT. Data are means ± average deviation (*error bars*) for 2–3 independent determinations. *, $p \leq 0.01$, with reference to the samples lacking lipid. *B–F*, elution profiles for the indicated CCTs concentrated without (*gray lines*) or with LPC (*green lines*) prior to application to a Superdex 200 FPLC column. The *panels* monitor the continuous $A_{280\ nm}$ in milliabsorbance units (*B–E*) and the LPC concentration in a subset of 1-ml elution fractions (*F*). The lipid profiles shown in *F* are also plotted alongside their respective CCT elution profiles in *B–D*. Molecular mass marker positions are indicated at the *top* of *B* with *arrows*. These constructs have N-terminal His tags and, with the exception of CCT-236 ΔJ, retain the NLS sequence.

dard (67 kDa) and the rest as heterogeneous high-mass aggregates. In the presence of lyso-PC, the protein elution profile converted to a single homogeneous peak with a mass of ~270 kDa, overlapping with the elution of the lipid (Fig. 5*B*). Whereas this construct binds to lipid micelles, it is only weakly activated by them (15), suggesting that the leash portion of domain M may participate in the creation of the active linker structure in a way that the AI helix alone cannot.

In the absence of lipid, CCT-236 eluted as a single, broad peak approximating a dimer, but upon the addition of micelles, the eluted complex size increased to ~220 kDa and co-eluted with phospholipid (Fig. 5*C*). The J-segment deletion mutant, CCT-236 Δ227–232, eluted as a ~70-kDa dimer in the absence of lipids. With the introduction of micelles, the elution profile shifted to a larger size, broadened, and co-eluted with lipid, confirming that the J segment is not solely responsible for the lipid interaction (Fig. 5*D*). However, CCT-212, lacking all of the αE_C and J segment, eluted as a 70-kDa dimer both in the absence and presence of micelles (Fig. 5*E*), suggesting that the αE_C contributes to the lipid interaction. The mass shifts in both the protein and lipid components (Fig. 5*F*) argue strongly for lyso-PC complex formation with CCTs containing the αEc/J, and provide evidence that a combination of the αE_C and J segment can form an independent, catalytically relevant membrane interaction. The lipid/protein molar ratios we measured in the higher mass-shifted peaks were ~70 for CCT-236 and CCT-236ΔJ, and ~115 for CCT-312Δ32. Using the mass shifts indicated in Fig. 5, we estimate an average of ~2 CCT dimers bound to a single lyso-PC particle. Although the interaction shown here is with a micellar lipid particle, it demonstrates that residues in the αE_C/J are lipophilic and thus would seek to embed in an accessible membrane surface.

Trp–dansyl-PE FRET supports a compact allosteric linker structure

The data in support of direct lipid interactions of the αE_C/J challenge the model shown in Fig. 6*E* with an extended structure for this region. If the αE helices bend to allow membrane interactions during the conversion from inactive to active CCT, the distance between the membrane and the catalytic domain would be shorter compared with the fully extended model. We estimate, using the solved structure of CCT_{sol} and estimating ≥10 Å for the span of the 12 amino acids of the J segment in a condensed form, that the distance between, for example, Phe-124 in loop L2 and the membrane surface in the fully extended αE, would be >30 Å. We used our set of single Trp variants to monitor FRET signals between the Trp donors and a lipid fluorescence acceptor, dansyl-PE, with a headgroup-attached fluorophore. The Forster length (R_0) for this FRET pair has been reported in the range of ~20–24 Å (45). A donor–acceptor separation of 30 Å would yield a FRET value of ~0.15 when R_0 = 22 Å.

In the first set of experiments, we monitored the increase in dansyl-PE fluorescence with increasing concentration of CCT

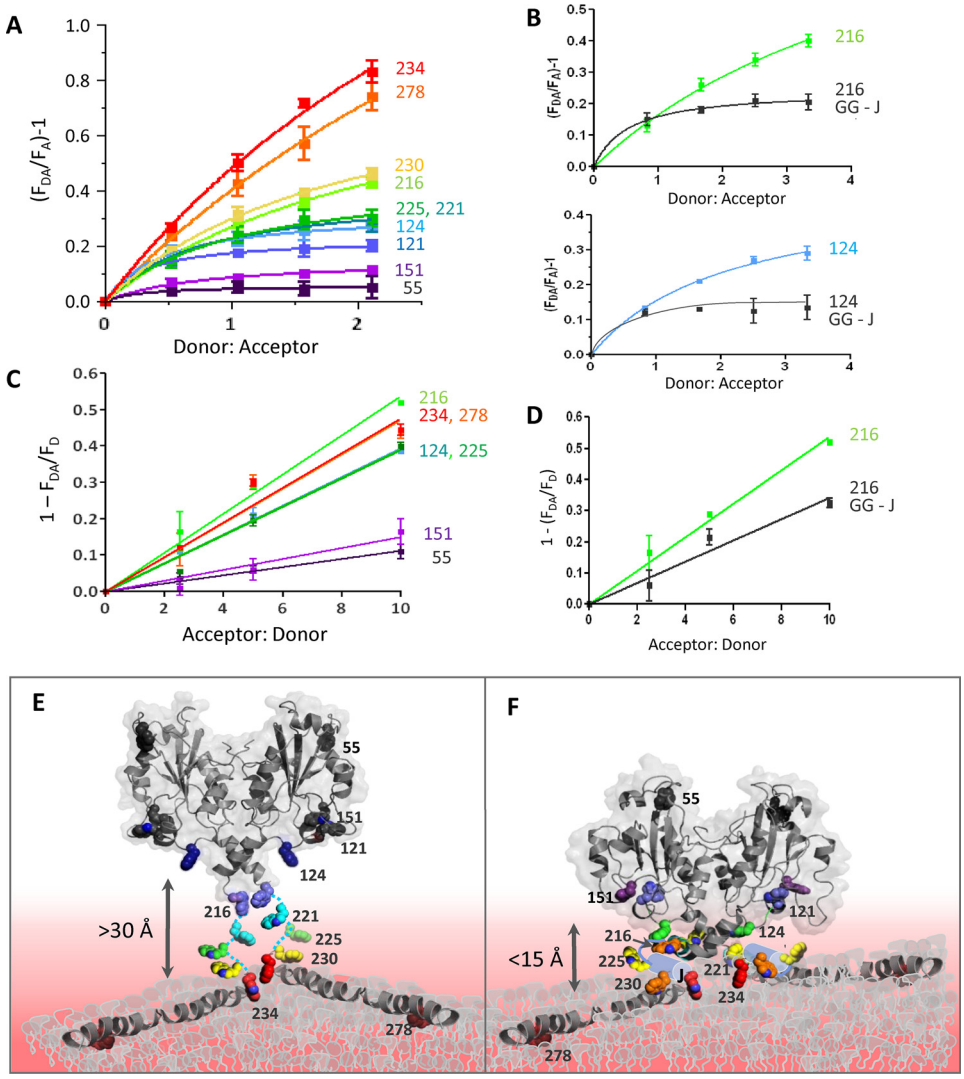

Figure 6. Trp to dansyl-PE FRET suggests a close membrane approach of the αE_C and active site. *A* and *B*, increases in dansyl-PE acceptor fluorescence with increasing [CCT]; *C* and *D*, decreases in Trp donor fluorescence with increasing [dansyl-PE]. Data in all *panels* are means ± range (*error bars*) of two independent determinations. Representative spectra are found in Figs. S4 and S5**.** Single-Trp constructs are derived from a CCT-312-His Δ12–16 background with native Trps removed (W151F; W278F). "W151" and "W278" retain the indicated single native Trp. *A*, samples contained CCT (0–4 μM) with a single Trp at the indicated residue and 100 μM vesicles (POPC/egg PG/dansyl-PE (50/48/1.8)). Trp was excited, and dansyl fluorescence was monitored at 520 nm. F_A, fluorescence at 520 nm when [CCT] = 0 μM; F_{DA}, intensity at 520 nm with increasing [CCT]. *B*, FRET from Trp-216 in αE_C or Trp-124 in L2 to dansyl-PE is reduced upon substitution of the WT linker with a glycine-rich sequence (GG-J; ^{227}GGGSGG^{232}). *C*, samples contained CCT (1 μM) with the indicated single Trp and 100 μM vesicles containing 50% POPC and the indicated mol % dansyl-PE balanced by egg PG. Trp was excited, and fluorescence was monitored at the peak wavelength for the Trp. F_D, Trp peak fluorescence in the presence of vesicles lacking dansyl-PE; F_{DA}, Trp fluorescence with increasing [dansyl-PE]. *D*, FRET between dansyl-PE and Trp-216 in the αE_C is reduced upon substitution of the WT J segment with a glycine-rich sequence (*GG-J*, ^{227}GGGSGG^{232}). *E* and *F*, two models for the allosteric linker structure in CCT_{mem}. *E*, fully extended αE_C/J. The model shows the positions of the Trp residues we monitored (*sphere representation*), *color-coded* to illustrate the degree of FRET expected in the fully extended form. *Black*, no FRET; *red*, maximum FRET. The *pink background* reflects the FRET gradient diminishing with distance from the membrane surface. No FRET is expected for residue 124 in loop L2 in this model of the allosteric linker. PDB entry 3HL4 was used for residues 40–216, and PDB entries 1PEI and 1PEH were used for the M helix (residues 236–288). The Trps missing from these structures (221, 225, 230, and 234) were placed manually. *F*, condensed αEc/J. The model shows the positions of the Trp residues *color-coded* to reflect the degree of FRET determined by experiment. Trp-124 in loop L2 is within FRET distance in this model, and the Trps in αEc/J occupy a nearly equivalent distance from the membrane. The CCT catalytic domain with bent αE helices is a snapshot obtained from an MD simulation of residues 40–223, without the constraining AI helices (14). The J segment is modeled as a *short lavender cylinder*. Trps not contained in the input structures were placed manually (Trp-225, -230, and -234).

and its Trp donor (Fig. 6*A*). The FRET curves were hyperbolic and saturated because as CCT was titrated into a fixed concentration of vesicles (100 μM), binding to the vesicles likely became restricted due to molecular crowding on the membrane surface. The lipid/protein ratio was only 25 at the highest donor/acceptor ratio, barely sufficient to solvate domain M (18). Despite this potential limitation, it is clear that Trp-278 in domain M, along with Trp-234, produced the highest FRET signals (Fig. 6*A*). The negative control, Trp-55, at the N-terminal of the catalytic domain, generated a very low FRET signal (0.05) that could reflect random collisions. Trp-151 near the active site and Trp-121/Trp-124 in loop L2 produced measurable FRET signals, suggesting an approach of these residues to the membrane interface that would not be possible with an extended allosteric linker conformation. The FRET signal produced by Trp-124 was especially intriguing, as it was similar in strength to the signals produced by Trp-221 in αE_C and Trp-225 in the J segment. FRET from Trp-216 was also surprisingly

strong, given its position near the start of the αE_C, stronger than Trp-221 at the C terminus of αE_C and similar to Trp-230 of the J segment. Therefore, the αE and J segment appear to lie along a similar plane with respect to the membrane surface.

To probe whether the strong FRET can be weakened by preventing αE-hinge bending, we attempted to straightjacket it by engineering a disulfide at nonconserved Ala-217 just C-terminal to the αE hinge. Recently, we showed that cysteines engineered at Ala-217 could be oxidized to produce ~50% disulfide-linked dimers, with accompanying inhibition of lipid activation (14). However, the Trp engineered at residue 216 to monitor FRET prevented the formation of a disulfide (<10%), so this approach was sidelined. Next, we tested the role of the native J segment sequence *versus* a nonspecific flexible sequence (^{227}GGGSGG^{232}) in stabilizing the structure of the allosteric linker that enables FRET between Trp at residue 216 (αE) or 124 (loop L2) and dansyl-PE in the membrane. With the glycine-rich J segment substitution, FRET from either Trp position was substantially decreased (Fig. 6*B*). Thus, the WT J sequence appears to facilitate the close membrane approach of the αE hinge and loop L2 of the catalytic domain.

We also measured FRET efficiency by monitoring the decrease in donor (Trp) fluorescence with increasing dansyl-PE concentration in the lipid vesicles (Fig. 6*C*). In this regime, the total lipid/protein ratio was constant (100 M/M; 2-fold in excess of that needed for complete solvation of domain M (18)), and this prevented FRET signal saturation due to vesicle surface crowding by CCT. These data illustrate a similar trend to that obtained when monitoring dansyl-PE, except Trp-216 produced the strongest FRET signal, even stronger than FRET from Trp-234 and Trp-278. Trp-124 in loop L2 and Trp-225 in the J segment produced similar FRET signals, suggesting that loop L2 hovers close to the membrane surface. The glycine-rich J mutation also reduced the FRET signal when monitoring Trp-216 fluorescence (Fig. 6*D*). Overall, the FRET data support a conformation for the αE_C/J during membrane binding that draws the catalytic domain close to the membrane surface (Fig. 6*F*).

Probing a mechanism for catalytic enhancement by a membrane-localized active site

We postulated that the bent αE would close off the opening to the active site and that this might enhance catalysis by reducing the water content of the active site. Fig. 7 (*A* and *B*) provides views of the active site opening of a CCT captured from one MD simulation (14). In Fig. 7*A*, the αE helices are both extended, revealing a large pocket at the base of the active site that becomes occupied by the αE_C after bending of the αE helices (Fig. 7*B*). Guca *et al.* (19) had found evidence for phosphocholine-independent PP_i production by a catalytically compromised K122A analog in the CCT from *P. falciparum*, suggesting that CTP hydrolysis might in some cases be a competing reaction for the cytidyl transfer reaction. A hydrolysis potential has never been established for CCT, but it could explain why, for example, the soluble form and CCT-236 have such high apparent K_m values for CTP. To determine whether these CCT forms can also catalyze CTP hydrolysis, we developed an assay where we compared the production of PP_i in the presence of phosphocholine (enabling the cytidyl transfer reaction) and in the absence of phosphocholine (no transfer). Details of the assay are provided in the supporting information and Fig. S7. PP_i generated in the latter condition can originate only from CTP hydrolysis (Fig. S8*A*). As expected, in the presence of lipids, we observed negligible PP_i generation in the absence of phosphocholine in full-length CCT and also CCT-236 (Fig. S8, *B* and *C*), indicating that hydrolysis was minimal. But in the absence of lipids, PP_i generation was also very low without phosphocholine addition and was elevated in the presence of phosphocholine (Fig. S8, *D* and *E*). The rate of PP_i generation by hydrolysis was only ~1% of the PP_i generation in the fully active enzyme via cytidyl transfer and was the same for reactions with and without lipid (0.22 nmol of PP_i/min/μg of CCT). Thus, hydrolysis was very inefficient in both CCT_{sol} and CCT_{mem}. We conclude that membrane binding does not stimulate cytidyl transfer by preventing CTP hydrolysis.

An alternative hypothesis for enhanced catalytic function is that a relatively anhydrous active site would strengthen the charge–charge interactions between enzyme and substrates. The CCT active site provides multiple amine-containing residues that overcome the repulsive negative charges between the substrates, CTP and phosphocholine (19, 20) (Fig. 7*A*). To probe this mechanism, we compared the ionic strength sensitivity of the activity of CCT_{mem} with that of CCT-236. According to our model, the former would have a solvent-shielded active site and would be less sensitive to ionic strength. We used lipid vesicles composed of zwitterionic phospholipids (DOPC/DOPE (2:3)) to circumvent an impact of ionic strength on membrane binding. In support of the solvent-shielding mechanism, the activity of CCT-236 was highly sensitive to increases in ionic strength, showing ~50% inhibition at 0.3 M, whereas the activity of CCT_{mem} was <10% inhibited at 0.3 M ionic strength (Fig. 7*C*).

Discussion

Recent molecular dynamics simulations indicated that without the constraining AI helices or membrane tether, the CCT allosteric linker (αE_C/J) samples many conformations (14, 15). In this work, we examined the hypotheses that the CCT allosteric linker (αE_C/J) interacts with the membrane surface, which could then guide its array of conformers into a preferred configuration for efficient catalysis. Two separate approaches provided evidence that the linker does indeed associate with membrane surfaces and that this association, at least with model membranes, can be independent of the M domain. In the process of trying to disrupt the membrane association of the J segment using mutagenesis, we came to the conclusion that both the αEc and J segment contribute to membrane interaction. We then probed the distance between the membrane surface and selective sites within the allosteric linker and catalytic domain by FRET. The distances were not compatible with an extended conformation for the linker, but rather suggested a condensed structure for αE_C/J. Mutations in the J segment decreased FRET between the membrane and sites near the αE hinge or active site.

These data combined with previous work suggest a sequence of steps accompanying the membrane binding and activation of

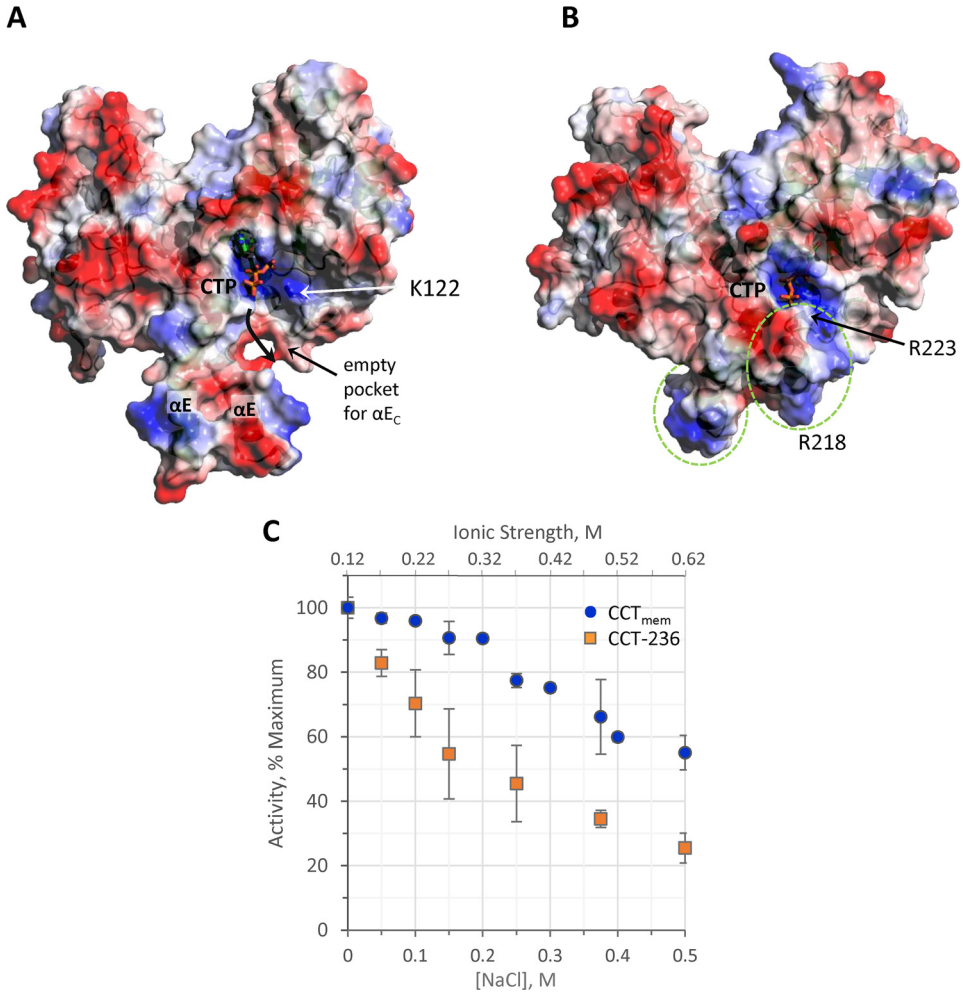

Figure 7. Membrane binding desensitizes the CCT active site to increased ionic strength. *A* and *B*, electrostatic surface of CCT with bound CTP, captured from one of 10 1-μs simulations (14). The simulations used CCT-312 Δ32 (PDB code 4MVC) with the AI helices removed as the starting structure (residues 40–223 are displayed). The surface was generated using a PyMOL function that does not account for solvent ion screening of the surface charge. *A*, snapshot from 20 ns into the simulation with extended αE helices, showing the large positively charged active site and empty pocket bounded by the αE helices and loop L2. The *arrow* indicates an exit route for CTP along a nonpolar groove. *B*, snapshot from 460 ns into the simulation, with bent αE helices, such as we propose for CCT$_{mem}$. The pocket is occupied by the αE$_C$ (*circled*), leading to partial burial of Lys-122 and CTP, and Arg-223 occupies the active-site entrance. *C*, CCT activity assays monitored [^{14}C]CDP-choline production at the indicated [NaCl] and ionic strength. CCT$_{mem}$ is full-length untagged CCTα bound to 0.25 mM DOPC/DOPE (2:3) vesicles, and His-CCT-236 was assayed without vesicles present. Data are means ± average deviation (*error bars*) of four independent trials.

CCT that begins with surface attraction of the positively charged leash region (residues ~236–271) of the M domain, dissociation of the AI helix from the four-helix complex, and membrane partitioning of the AI and leash as a folded helix. AI dissociation is followed by bending of the αE helix at its hinge and conformational sampling of the αE$_C$ and J segment guided by a fully bound M-helix. The acquisition of a bent, compact structure for the allosteric linker creates a lid that partly covers the opening to the active site and draws it close to the membrane surface. The result is generation of a more anhydrous environment for efficient catalysis.

The αE$_C$/J is more than an extension of the M domain or an unstructured tether

No structural studies of lipid-regulated CCTs have provided the favored conformation of the αE$_C$/J in the active, membrane-bound form. An initial possibility, suggested by the Br-PC quenching, was that that the αE$_C$/J segment is simply an amphipathic helical extension of domain M. This is not likely for several reasons. First, the helical hydrophobic moment (21, 22) of the αE$_C$/J is only 0.08 compared with a value of 0.36 for the N-terminal 18 residues of domain M (residues 234–251). Second, Br-PC quenching of Trps in the αE$_C$/J was modest compared with Trps within the M domain and was more effective with the surface-proximal bromine (6,7-Br-PC) rather than deeper bromo positions. This suggests that the J segment is not embedded to the extent of domain M. The small vesicles we used have a highly disordered surface that enables contact between acyl chains and superficially situated peptides. Third, the high sensitivity of CCT activity to mutation in the J segment is not expected if the linker is solely a membrane-binding domain. For example, the L230W or V232W mutations in the J segment should benefit CCT activation as they would enhance membrane partitioning, but they devastated CCT activity (13).

Our data also rule out the αE$_C$/J as either an unstructured tether or an unbroken extended α-helix between domains. The complete loss of activity upon substitution with the glycine-rich J segment argues against a mere tethering function. That the

sequence conservation is as high as the catalytic domain is also hard to rationalize with an unstructured tether, but it fits with a folded structure making intramolecular contacts that are regulated by membrane binding. FRET between Trps within the αE_C/J and dansyl-PE in the membrane did not abate in relation to their sequence distance toward the N terminus. Rather, the FRET signals were similar, suggesting that they lie roughly within a single plane parallel to the membrane surface, perhaps folding into a condensed structure, with the J segment more penetrant of the surface, based on Br-PC quenching. The FRET data also position Trp-124 in loop L2 of the active site at a similar distance from the membrane surface as Trp-221 (αE_C) and Trp-225 (J segment), which is completely at odds with an extended helical or unstructured αE_C/J segment (Fig. 6, *E* and *F*).

Multiple conserved residues throughout the αE_C/J likely contribute to membrane interactions

To assess whether the allosteric linker–membrane interaction is required to transduce signals from domain M to the catalytic domain, we tried to disrupt the interaction by mutagenesis. Surprisingly, none of the mutations designed to disrupt potential hydrophobic, electrostatic, or aromatic interactions were effective in dislodging the J segment from the membrane, as monitored by Br-PC quenching potential toward a Trp in the J segment. A limitation of these experiments was that the engineered tryptophans could have a stronger interfacial driving force than the native tyrosine or leucine that they replace (23, 24) and could artificially forge linker–membrane interactions not available to the WT CCT. However, gel filtration analysis of lipid interaction, which did not rely on engineered tryptophans, also revealed that deletion of the J segment from CCT-236 was not sufficient to abolish the lipid interaction, whereas deletion of the entire allosteric linker (CCT-212) destroyed the lipid interaction. One explanation consistent with these results is that the membrane association of the linker relies on multiple sites dispersed throughout the entire αE_C/J sequence including, but not exclusive to, the sites targeted for mutation. The lipid interaction of CCT-236, observed by the two independent methods, demonstrates the intrinsic affinity of the αE_C/J segment independent of domain M. The CCT-236 membrane affinity is clearly weaker than that of CCT with the M domain intact. For example, we can isolate by ultracentrifugation a CCT-312 vesicle complex, but not a CCT-236 vesicle complex (25, 26). In cells, oleic acid induces translocation of full-length CCT, but not CCT-236, to intranuclear membranes (11). Moreover, the lipid interaction of the αE_C/J in CCT-236 is much less effective in promoting conformations and interactions productive for catalysis than when the αE_C/J is linked to a membrane-embedded M domain, hence the ~20-fold lower catalytic efficiency (13).

Direct interactions between the αE_C J segment, and lipid may direct the folding of the allosteric linker on the membrane surface

Whereas the allosteric linker mutations we created did not abrogate membrane interaction, they did abolish activation, suggesting that these residues may participate in creating a tertiary structure for the allosteric linker compatible with high catalytic activity. The mutations may have disrupted direct interactions between the αE_C and J segment, even though the allosteric linker was still adsorbed onto the membrane surface. In our model, the αE_C/J forges a network of protein and lipid interactions that are promoted by the membrane partitioning of the M domain, and this network underlies signal transduction between the M and C domains. Substitution with a glycine-rich J segment reduced FRET between Trp-216 and dansyl-PE, and this was observed when we monitored either dansyl or Trp fluorescence. This supports a role for the J segment in stabilizing the compact structure of the allosteric linker. Bent helix conformations generated during simulations expose a hydrophobic groove between the two αEc helices that could accommodate the J segment or, alternatively, dock onto the membrane.

Reduced solvent exposure of residues Tyr-213 and Tyr-216 in CCT_{mem} (13) suggested a folded structure for the αE_C. In the bent αE visualized in the MD simulations, the αE_C interacts with loop L2, but the αE_C could also forge interactions with the J segment on the membrane surface. This idea is supported by the obliteration of lipid-induced activity upon introducing bulky hydrophobic residues in the allosteric linker (L221W, L230W, and V232W) that could prevent close association of the two segments (13). We analyzed CCT sequence alignments from a wide range of eukaryotic phyla for coupled residue substitutions in the αE_C and J segment that might imply an interaction between the two residues. One striking substitution occurred in Ascomycota fungus sequences. Position 221 in the αE_C, a leucine in most species, is mutated to a phenylalanine, and in concert, position 225 in the J segment is changed from tyrosine to alanine (Fig. S6). The co-evolution of the L221F/Y225A switch suggests that a mutation to the bulky Phe at residue 221 is not compatible with the bulky Tyr at residue 225, but a Y225A mutation would alleviate steric clash between two putative interacting sites. In support of this interaction, an L221W mutation severely inhibited CCT activity, whereas a Y225W mutation did not.

Tyr-216 appears to have an outsized role in the allosteric transitions. It can be replaced by Phe or Trp without impairing activity, but not alanine or cysteine (13). Of all the residues we probed, it shows the largest protection from solvent and a large dequenching upon membrane binding and is located very close to the membrane surface, based on the FRET analyses.

Attempts to solve the crystal structure of CCT bound to micelles have been unsuccessful. However, a previously described 8 Å structure of a CCT tetramer provides a clue for the conformational preference of the J segment. In this structure, the two M helices of one dimer extend from the αE and interact with two M helices of another dimer to form a >75-Å four-helix bundle (PDB entry 4MVD) (15). The electron density defines the residues comprising the αE_C and J segment as helical, linked by a ~75° turn at ^{223}RGY^{225} in two of the four chains (15). We used the rat CCTα sequence of the αE_C/J as a query to search the PDB for sequence matches. We obtained just six hits that contained exact matches of 4–7 contiguous residues of the J segment sequence (Fig. S9). The preferred conformation of the J segment from this limited set is a helix or a turn-helix that

docks into clefts formed by other helices. Such a conformation fits well with the FRET data supporting a compact, lipid-associating structure, and the helix-turn-helix preference is reflected in our model for the allosteric linker in Fig. 6*F*.

How could a compact allosteric linker aid catalysis?

Bending of the αE helices positions conserved residues of one face of the αE_C within close proximity of the epicenter of CCT catalysis at loop L2. The opposite face of the αE_C helix could orient toward the J segment near the membrane interface, forging both protein and lipid interactions (Fig. 6*F*). Both sets of interactions may be important for stabilizing an αE_C helical structure, compensating for contacts lost during dissociation of the AI helices. The folded allosteric linker may play a fundamental role in accelerating catalysis by creating a relatively anhydrous milieu for the cytidyl-transfer reaction as it covers the large active site entrance and pulls the active site close to the membrane. The protection of Trp-151 in the active site from acrylamide quenching upon membrane binding (13) is in agreement with this proposal. We ruled out the possibility that the enzyme can also catalyze CTP hydrolysis in competition with cytidyl transfer, where a water molecule would substitute for the phosphocholine in the reaction. But there is another more basic advantage of water exclusion. In the cytidyl-transfer reaction, both the nucleophilic phosphate and the α-phosphate target have strong repulsive negative charge. The enzyme donates several basic groups to counter that charge (20), and dehydration of the active site cleft would strengthen the charge–charge interactions between enzyme and substrates. This is a fundamental mechanistic basis for lid closure over active sites and can yield rate enhancements of orders of magnitude (27–29). In support of this mechanism, we found that the activity of the catalytic fragment, CCT-236, with its open active site, was much more sensitive to inhibition by raising the ionic strength of the medium than was membrane-bound CCT. This simple test has been used to show the involvement of basic residues in electrostatic facilitation of superoxide dismutase using superficial sites sensitive to ionic strength and one site deep in the active site that is resistant (30, 31). The sensitivity differences of the two CCT forms cannot be ascribed to structure destabilization of CCT-236 by high salt concentration, as the crystals used to solve its structure were grown in 1.2 M salt. The structure of the CCT containing the AI helix of the M domain was obtained from crystals grown in 0.2 M salt, and both structures provide catalytic domains that superimpose upon each other (15). MD simulations revealed that upon bending of the αE helices, the basic αEc residues, Arg-218, Arg-219, and especially Arg-223, made frequent excursions into the active site and made contact with the CTP γ-phosphate (14) (Fig. 7*B*). Possibly, one or more of these arginines contribute to charge facilitation in the active site at some step in the catalytic cycle. In support of this, Arg-223 is mutated to a serine in a CCTα allele linked to the rare human skeletal and retinal disease, SMD-CRD (32), with a consequent 16-fold drop in k_{cat}/K_m (33).

Why then would the unregulated GCT have high catalytic efficiency despite lacking the αE_C/J? Loop L2 may provide a substitute device in GCT, as it is longer and more flexible and is extremely basic, with 3 lysines and 1 histidine in contrast to just 1 lysine at residue 122 in the shorter mammalian CCT loop L2. Two of the GCT lysines have been probed, showing that they are critical for activity (34). The extra positive charge may compensate for the higher water density in the active site during the reaction.

The AI helices inhibit catalytic function by partly occluding the active site entrance. Is it then incongruous to propose that closing off the active site by the αE_C promotes activity? Not if the interactions have different time scales and consequences. The MD simulations showed that the contact between the AI and loop L2 of the active site was relatively stable and steered the catalytic lysine away from substrate. Because the entrance to the active site must be open for substrate entry/product release, we envision that the allosteric linker might sample different conformations during a catalytic cycle, with a bent αE and membrane-proximal active site most prominent after substrates are bound and prior to product release. The present FRET analysis of interdomain distance was done with an empty active site. Future work should explore the interdomain distance with different ligands occupying the active site.

In summary, part of the CCT inactivation mechanism involves immobilization of the allosteric linker using a portion of the membrane-binding domain (the AI helix). Displacement of the AI by membrane engagement frees the linker to sample many new conformations, but the membrane tether is likely to dictate a restricted ensemble. Moreover, the intrinsic affinity of the allosteric linker for the membrane interface will promote a hierarchical folding pathway leading to a condensed linker structure that draws the active site toward the membrane and away from bulk solvent.

Several aspects of the mechanism of CCT activation by its allosteric linker may be shared with other membrane-associated enzymes, most notably another enzyme of phospholipid metabolism, neutral sphingomyelinase (nSMase2). The catalytic domain of nSMase2 is linked to an integral membrane binding domain by a juxtamembrane region that, like the αE_C/J of CCT, is triggered to fold upon interaction with anionic phospholipids, mediates contact between the catalytic domain and the membrane-binding domain, and induces active site restructuring to facilitate substrate (sphingomyelin) access (35, 36). Group IVA iPLA2 has no discrete membrane-binding domain and no linker, but two loops flanking the active site opening for PC interact with the membrane surface to facilitate opening of the cleft in the catalytic domain for substrate (37). More broadly, small GTPases like H-Ras and Arf1 can adopt different orientations with respect to the membrane surface that display different states of GTPase activity. These orientations are dictated by the fluctuating ensemble of conformers for the membrane-interacting linker (HVR) joining the GTPase domain to the lipidated C-terminal anchor (38). Last, membrane-bound kinases such as the EGF receptor (39, 40) also use refolding/reorientation of membrane-interacting linkers bridging two domains to induce substantial shifts in the quaternary structure and activity of the enzyme domain.

Experimental procedures

Construction, expression, and purification of CCTs

The materials and methods for construct preparation were described in the companion paper (13). In addition to the many CCT forms described in that paper that were used in the present work, we prepared additional mutants delineated in Table S1. CCT-312 variants contained a C-terminal His tag for purification (^{313}LEHHHHHH^{320}) and a deletion of the nuclear localization signal (NLS; residues 12–16) to prevent vesicle aggregation, which interferes with fluorescence analysis (13). CCT-212, CCT-236, and CCT-312(Δ32) had N-terminal His tags (MGSSH$_6$SSGLVPRGSH) and intact NLS sequences.

CCT enzyme activity

Monitoring [^{14}C]CDP-choline production—The specific activity was determined as described previously (33, 41). For the standard assay, optimal for WT CCT, the concentrations of CTP and phosphocholine in the assay were 8 and 1.6 mM, respectively. Kinetic constants were determined by varying the CTP concentration from 0 to 16 mM using a fixed (2 mM) concentration of phosphocholine. Sonicated lipid vesicles were prepared as described previously (41), except the suspensions were sonicated for 15 min on 50% output and were centrifuged for 4 min at 13,000 × *g* to remove titanium debris introduced by the sonicator probe. The vesicles were stored under argon at 4 °C and used within ~2 days. The vesicle lipid compositions are described in the figure legends. For probing the effects of NaCl concentration on CCT activity, the ionic strength was calculated as follows,

$$I = 0.5\left(\sum(c_i Z_i^2)\right) \quad \text{(Eq. 1)}$$

for all anions and cations, where *c* represents molar concentration and *z* is charge. The ionic strength was 0.12 M based on buffer, substrate, and cofactor contributions. NaCl was the added variable. The substrate CTP was added to the enzyme either before or after introduction of the salt (NaCl), with no significant differences in the activity outcome.

Monitoring unlabeled PP$_i$ production—This novel assay is described in the supporting information.

Thermal denaturation using SYPRO Orange

The transition temperature for unfolding was measured using the hydrophobic dye SYPRO Orange (Invitrogen, Molecular Probes), as described (33).

Quenching of single-tryptophan CCT variants by dibrominated PC

Nonquenching vesicles contained egg PG/POPC (1:1), and quenching vesicles contained egg PG/dibrominated PC (1:1) with bromines conjugated to carbons 6,7, 9,10, or 11,12. The perturbation to the bilayer by dibromo-PC substitution is similar to that of a double bond (42). The lipid concentration dependence for CCT-312 activation and the maximal activity was nearly identical for vesicles composed of 50% egg PG and either 50% 11,12-diBr-PC or 50% POPC. Samples (300 μl) were prepared by mixing 3 μM CCT and 450 μM vesicles in 10 mM Tris, pH 7.4, 150 mM NaCl, 2 mM DTT and incubating for 5 min at room temperature. Fluorescence scans were measured at 20 °C on a Cary Eclipse fluorescence spectrophotometer using the parameters for Trp fluorescence described by Taneva *et al.* (13). Duplicate scans were averaged, and lipid-only blanks were subtracted to generate corrected fluorescence emission spectra. The fluorescence intensity for each spectrum was recorded at the peak emission wavelength average for each set of Trp variants.

Superdex-200 gel filtration of CCT-micelle complexes

The CCT preparation was mixed with a 175–180-fold molar excess of LPC (16:0) in 10 mM Tris, pH 8, 300 mM NaCl, 2 mM DTT, and concentrated using an Amicon Ultra-spin filter (30-kDa cutoff) at 4000 rpm to a protein concentration of 150–300 μM. Samples (0.4-ml volume) were applied to a Superdex 200 10/300 FPLC gel-filtration column (24-ml bead volume) pre-equilibrated with 10 mM Tris, pH 8, 0.1 M NaCl, and 2 mM DTT. The column had been precalibrated with the mass standards: dextran, >2000 kDa; ferritin, 440 kDa; catalase, 220 kDa; BSA, 67 kDa; and RNase, 13.7 kDa. The FPLC-controlled flow rate was 0.4 ml/min, and 1-ml volume fractions were collected. For each elution fraction, lipid phosphorus (43) and protein concentration (44) were measured in duplicate.

Tryptophan–dansyl-PE FRET

Monitoring increases in dansyl-PE fluorescence—Sonicated vesicles were prepared containing POPC/egg PG/dansyl-PE (50:48:1.8). Samples (300 μl) were prepared by mixing 100 μM vesicles with 0–4 μM CCT in 10 mM Tris, pH 7.4, 150 mM NaCl, 2 mM DTT and incubating for 5 min at room temperature. In pilot experiments, we explored the CCT and lipid concentrations and percentage dansyl-PE vesicle compositions that produced optimal FRET signals, with maximal signal/noise ratio, lack of interference by lipid vesicle light scattering, and differentiation among the various Trp sites. The optimal parameters were a donor/acceptor ratio of up to 4:1 and lipid/protein ratios of 100 to 25. The excitation wavelength was 280 nm to maximize donor tryptophan excitation, and the emission was scanned from 290 to 590 nm. The remainder of the fluorimeter settings were identical to the Trp quenching experiments. The FRET efficiency was calculated from the intensity increase at 520 nm (dansyl emission peak) as follows,

$$(F_{DA}/D_A) - 1 \quad \text{(Eq. 2)}$$

where F_{DA} is the acceptor fluorescence in the presence of donor and F_A is the acceptor fluorescence in the absence of donor. The plot of the FRET signal *versus* D/A molar ratio was fit to a one-site binding hyperbola fit using GraphPad Prism 4.

The fluorescence values at 520 nm for the FRET calculation were taken directly from the raw spectra. To assess whether the increases in dansyl fluorescence with increasing [CCT] included a contribution of the CCT Trp fluorescence, we monitored the fluorescence signal at 520 nm of samples containing 0–4 μM CCT but no dansyl-PE vesicles. Signal increases were negligible up to a 4 μM concentration of each single-Trp CCT, and this background signal was not subtracted.

An important caveat to consider is that dansyl fluorescence increases could be affected by differences in intensity and peak wavelengths of the donor that vary based on the environment of different Trp sites. However, all of the native and engineered Trps emitted near the dansyl absorbance maximum of 336 nm. Moreover, the Forster distance, $R_{0,}$ is not highly dependent on spectral overlap or donor quantum yield (16), and thus FRET efficiency values would not vary significantly among Trps based solely on small blue shifts and intensity differences. The main determinant of FRET in these experiments is the donor–acceptor distance.

Monitoring decreases in tryptophan fluorescence—Sonicated vesicles were prepared containing 0, 2.5, 5, or 10% dansyl-PE in 50% POPC, balanced with egg PG. Samples (300 μl) were prepared by mixing 100 μM vesicles with 1 μM CCT in 10 mM Tris, pH 7.4, 150 mM NaCl, 2 mM DTT and incubating for 5 min at room temperature. The excitation wavelength was 290 nm to minimize tyrosine excitation, and the emission was scanned from 300 to 420 nm. The remainder of the fluorimeter settings were identical to the Trp quenching experiments. Two scans were averaged, and lipid blank scans were subtracted to generate corrected fluorescence spectra. The FRET efficiency was calculated from intensity changes at the peak wavelength for each Trp mutant as follows,

$$1 - (F_{DA}/F_D) \quad \text{(Eq. 3)}$$

where F_{DA} is the donor fluorescence in the presence of acceptor and F_D is the donor fluorescence in the absence of acceptor. The plot of $1 - (F_{DA}/F_D)$ *versus* the acceptor/donor molar ratio was fit linearly using GraphPad Prism 4.

Author contributions—D. G. K., J. L., S. G. T., and R. B. C. conceptualization; D. G. K., J. L., S. G. T., and R. B. C. data curation; D. G. K., J. L., S. G. T., and R. B. C. formal analysis; D. G. K. and R. B. C. supervision; D. G. K. and R. B. C. funding acquisition; D. G. K., J. L., S. G. T., and R. B. C. validation; D. G. K., J. L., S. G. T., and R. B. C. investigation; D. G. K., J. L., S. G. T., and R. B. C. visualization; D. G. K., J. L., S. G. T., and R. B. C. methodology; D. G. K., J. L., S. G. T., and R. B. C. writing-original draft; D. G. K. and R. B. C. project administration; D. G. K., J. L., S. G. T., and R. B. C. writing-review and editing.

Acknowledgments—We are grateful to Jillian Smith for the original discovery that CCT-236 is activated by lysolipids. We thank Dr. Tom Claydon for discussions of the FRET data, Dr. Peter Tieleman for valuable comments on the manuscript, and Cameron Proceviat for his contribution early in the project.

References

1. Ma, B., Tsai, C. J., Haliloğlu, T., and Nussinov, R. (2011) Dynamic allostery: linkers are not merely flexible. *Structure* **19,** 907–917 CrossRef Medline
2. Akimoto, M., Selvaratnam, R., McNicholl, E. T., Verma, G., Taylor, S. S., and Melacini, G. (2013) Signaling through dynamic linkers as revealed by PKA. *Proc. Natl. Acad. Sci. U.S.A.* **110,** 14231–14236 CrossRef Medline
3. English, C. A., Sherman, W., Meng, W., and Gierasch, L. M. (2017) The Hsp70 interdomain linker is a dynamic switch that enables allosteric communication between two structured domains. *J. Biol. Chem.* **292,** 14765–14774 CrossRef Medline
4. Kim, C., Xuong, N. H., and Taylor, S. S. (2005) Crystal structure of a complex between the catalytic and regulatory (RIα) subunits of PKA. *Science* **307,** 690–696 CrossRef Medline
5. Liu, J., and Nussinov, R. (2010) Molecular dynamics reveal the essential role of linker motions in the function of cullin-RING E3 ligases. *J. Mol. Biol.* **396,** 1508–1523 CrossRef Medline
6. Cornell, R. B. (2016) Membrane lipid compositional sensing by the inducible amphipathic helix of CCT. *Biochim. Biophys. Acta* **1861,** 847–861 CrossRef Medline
7. Aitchison, A. J., Arsenault, D. J., and Ridgway, N. D. (2015) Nuclear-localized CTP:phosphocholine cytidylyltransferase α regulates phosphatidylcholine synthesis required for lipid droplet biogenesis. *Mol. Biol. Cell* **26,** 2927–2938 CrossRef Medline
8. Cornell, R., and Antonny, B. (2018) CCTα commands phospholipid homeostasis from the nucleus. *Dev. Cell* **45,** 419–420 CrossRef Medline
9. Craddock, C.P., Adams, N., Bryant, F.M., Kurup, S., and Eastmond, P.J. (2016) Phosphatidic acid phosphohydrolase Regulates Phosphatidylcholine Biosynthesis in Arabidopsis by Phosphatidic Acid-Mediated Activation of CTP: phosphocholine cytidylyltransferase activity. *Plant Cell* **27,** 1251–1264 CrossRef Medline
10. Haider, A., Wei, Y. C., Lim, K., Barbosa, A. D., Liu, C. H., Weber, U., Mlodzik, M., Oras, K., Collier, S., Hussain, M. M., Dong, L., Patel, S., Alvarez-Guaita, A., Saudek, V., Jenkins, B. J., *et al.* (2018) PCYT1A regulates phosphatidylcholine homeostasis from the inner nuclear membrane in response to membrane stored curvature elastic stress. *Dev. Cell* **45,** 481–495.e8 CrossRef Medline
11. Lagace, T. A., and Ridgway, N. D. (2005) The rate-limiting enzyme in phosphatidylcholine synthesis regulates proliferation of the nucleoplasmic reticulum. *Mol. Biol. Cell* **16,** 1120–1130 CrossRef Medline
12. Cornell, R. B., and Ridgway, N. D. (2015) CTP:phosphocholine cytidylyltransferase: function, regulation, and structure of an amphitropic enzyme required for membrane biogenesis. *Prog. Lipid Res.* **59,** 147–171 CrossRef Medline
13. Taneva, S. G., Lee, J., Knowles, D. G., Tishyadhigama, C., Chen, H., and Cornell, R. B. (2019) Interdomain communication in the phosphatidylcholine-regulatory enzyme, CCTα, relies on a modular αE helix. *J. Biol. Chem.* **294,** XXXXX–XXXXX CrossRef
14. Ramezanpour, M., Lee, J., Taneva, S. G., Tieleman, D. P., and Cornell, R. B. (2018) An auto-inhibitory helix in CTP:phosphocholine cytidylyltransferase hijacks the catalytic residue and constrains a pliable, domain-bridging helix pair. *J. Biol. Chem.* **293,** 7070–7084 CrossRef Medline
15. Lee, J., Taneva, S. G., Holland, B. W., Tieleman, D. P., and Cornell, R. B. (2014) Structural basis for autoinhibition of CTP:phosphocholine cytidylyltransferase (CCT), the regulatory enzyme in phosphatidylcholine synthesis, by its membrane-binding amphipathic helix. *J. Biol. Chem.* **289,** 1742–1755 CrossRef Medline
16. Lakowicz, J. R. (2006) *Principles of Fluorescence Spectroscopy*, 3rd Ed., pp. 278–279. Springer, New York
17. Johnson, J. E., and Cornell, R. B. (1994) Membrane-binding amphipathic α-helical peptide derived from CTP:phosphocholine cytidylyltransferase. *Biochemistry* **33,** 4327–4335 CrossRef Medline
18. Taneva, S. G., Lee, J. M., and Cornell, R. B. (2012) The amphipathic helix of an enzyme that regulates phosphatidylcholine synthesis remodels membranes into highly curved nanotubules. *Biochim. Biophys. Acta* **1818,** 1173–1186 CrossRef Medline
19. Guca, E., Nagy, G. N., Hajdú, F., Marton, L., Izrael, R., Hoh, F., Yang, Y., Vial, H., Vértessy, B. G., Guichou, J.-F., and Cerdan, R. (2018) Structural determinants of the catalytic mechanism of Plasmodium CCT, a key enzyme of malaria lipid biosynthesis. *Sci. Rep.* **8,** 11215 CrossRef Medline
20. Lee, J., Johnson, J., Ding, Z., Paetzel, M., and Cornell, R. B. (2009) Crystal structure of a mammalian CTP:phosphocholine cytidylyltransferase catalytic domain reveals novel active site residues within a highly conserved nucleotidyltransferase fold. *J. Biol. Chem.* **284,** 33535–33548 CrossRef Medline
21. Eisenberg, D., Weiss, R. M., and Terwilliger, T. C. (1982) The helical hydrophobic moment: a measure of the amphiphilicity of a helix. *Nature* **299,** 371–374 CrossRef Medline

22. Gautier, R., Douguet, D., Antonny, B., and Drin, G. (2008) HELIQUEST: a web server to screen sequences with specific α-helical properties. *Bioinformatics* **24,** 2101–2102 CrossRef Medline
23. MacCallum, J. L., Bennett, W. F., and Tieleman, D. P. (2008) Distribution of amino acids in a lipid bilayer from computer simulations. *Biophys. J.* **94,** 3393–3404 CrossRef Medline
24. Wimley, W. C., and White, S. H. (1996) Experimentally determined hydrophobicity scale for proteins at membrane interfaces. *Nat. Struct. Biol.* **3,** 842–848 CrossRef Medline
25. Dennis, M. K., Taneva, S. G., and Cornell, R. B. (2011) The intrinsically disordered nuclear localization signal and phosphorylation segments distinguish the membrane affinity of two cytidylyltransferase isoforms. *J. Biol. Chem.* **286,** 12349–12360 CrossRef Medline
26. Taneva, S., Dennis, M. K., Ding, Z., Smith, J. L., and Cornell, R. B. (2008) Contribution of each membrane binding domain of the CTP:phosphocholine cytidylyltransferase-α dimer to its activation, membrane binding, and membrane cross-bridging. *J. Biol. Chem.* **283,** 28137–28148 CrossRef Medline
27. Hammes, G. G. (2002) Multiple conformational changes in enzyme catalysis. *Biochemistry* **41,** 8221–8228 CrossRef Medline
28. Malabanan, M. M., Amyes, T. L., and Richard, J. P. (2010) A role for flexible loops in enzyme catalysis. *Curr. Opin. Struct. Biol.* **20,** 702–710 CrossRef Medline
29. Vandemeulebroucke, A., De Vos, S., Van Holsbeke, E., Steyaert, J., and Versées, W. (2008) A flexible loop as a functional element in the catalytic mechanism of nucleoside hydrolase from *Trypanosoma vivax*. *J. Biol. Chem.* **283,** 22272–22282 CrossRef Medline
30. Cudd, A., and Fridovich, I. (1982) Electrostatic interactions in the reaction mechanism of bovine erythrocyte superoxide dismutase. *J. Biol. Chem.* **257,** 11443–11447 Medline
31. Klapper, I., Hagstrom, R., Fine, R., Sharp, K., and Honig, B. (1986) Focusing of electric fields in the active site of Cu-Zn superoxide dismutase: effects of ionic strength and amino-acid modification. *Proteins* **1,** 47–59 CrossRef Medline
32. Hoover-Fong, J., Sobreira, N., Jurgens, J., Modaff, P., Blout, C., Moser, A., Kim, O. H., Cho, T. J., Cho, S. Y., Kim, S. J., Jin, D. K., Kitoh, H., Park, W. Y., Ling, H., Hetrick, K. N., *et al.* (2014) Mutations in PCYT1A, encoding a key regulator of phosphatidylcholine metabolism, cause spondylometaphyseal dysplasia with cone-rod dystrophy. *Am. J. Hum. Genet.* **94,** 105–112 CrossRef Medline
33. Cornell, R. B., Taneva, S. G., Dennis, M. K., Tse, R., Dhillon, R. K., and Lee, J. (2019) Disease-linked mutations in the phosphatidylcholine regulatory enzyme CCTα impair enzymatic activity and fold stability. *J. Biol. Chem.* **294,** 1490–1501 CrossRef Medline
34. Pattridge, K. A., Weber, C. H., Friesen, J. A., Sanker, S., Kent, C., and Ludwig, M. L. (2003) Glycerol-3-phosphate cytidylyltransferase: structural shanges induced by binding of CDP-glycerol and the role of lysine residues in catalysis. *J. Biol. Chem.* **278,** 51863–51871 CrossRef Medline
35. Airola, M. V., Shanbhogue, P., Shamseddine, A. A., Guja, K. E., Senkal, C. E., Maini, R., Bartke, N., Wu, B. X., Obeid, L. M., Garcia-Diaz, M., and Hannun, Y. A. (2017) Structure of human nSMase2 reveals an interdomain allosteric activation mechanism for ceramide generation. *Proc. Natl. Acad. Sci. U.S.A.* **114,** E5549–E5558 CrossRef Medline
36. Shanbhogue, P., Hoffmann, R. M., Airola, M. V., Maini, R., Hamelin, D. J., Garcia-Diaz, M., Burke, J. E., and Hannun, Y. A. (2019) The juxtamembrane linker in neutral sphingomyelinase-2 functions as an intramolecular allosteric switch that activates the enzyme. *J. Biol. Chem.* **294,** 7488–7502 CrossRef Medline
37. Mouchlis, V. D., Bucher, D., McCammon, J. A., and Dennis, E. A. (2015) Membranes serve as allosteric activators of phospholipase A2, enabling it to extract, bind, and hydrolyze phospholipid substrates. *Proc. Natl. Acad. Sci. U.S.A.* **112,** E516–E525 CrossRef Medline
38. Prakash, P., and Gorfe, A. A. (2017) Membrane orientation dynamics of lipid-modified small GTPases. *Small GTPases* **8,** 129–138 CrossRef Medline
39. Endres, N. F., Das, R., Smith, A. W., Arkhipov, A., Kovacs, E., Huang, Y., Pelton, J. G., Shan, Y., Shaw, D. E., Wemmer, D. E., Groves, J. T., and Kuriyan, J. (2013) Conformational coupling across the plasma membrane in activation of the EGF receptor. *Cell* **152,** 543–556 CrossRef Medline
40. Maeda, R., Sato, T., Okamoto, K., Yanagawa, M., and Sako, Y. (2018) Lipid-protein interplay in dimerization of juxtamembrane domains of epidermal growth factor receptor. *Biophys. J.* **114,** 893–903 CrossRef Medline
41. Sohal, P. S., and Cornell, R. B. (1990) Sphingosine inhibits the activity of rat liver CTP:phosphocholine cytidylyltransferase. *J. Biol. Chem.* **265,** 11746–11750 Medline
42. McIntosh, T. J., and Holloway, P. W. (1987) Determination of the depth of bromine atoms in bilayers formed from bromolipid probes. *Biochemistry* **26,** 1783–1788 CrossRef Medline
43. Bartlett, G. R. (1959) Phosphorus assay in column chromatography. *J. Biol. Chem.* **234,** 466–468 Medline
44. Bradford, M. M. (1976) A rapid and sensitive method for the quantitation of microgram quantities of protein utilizing the principle of protein-dye binding. *Anal. Biochem.* **72,** 248–254 CrossRef Medline
45. Lakowicz, J. R. (2006) *Principles of Fluorescence Spectroscopy*, 3rd Ed., pp. 468, Springer, New York